Presence of antisite disorder and its characterization in the predicted half-metal Co_2MnSi

M. P. Raphael,[1] B. Ravel,[1] Q. Huang,[2] M. A. Willard,[1] S. F. Cheng,[1] B. N. Das,[1] R. M. Stroud,[1] K. M. Bussmann,[1] J. H. Claassen,[1] and V. G. Harris[1]

[1]*U.S. Naval Research Laboratory, Washington, DC 20375*

[2]*National Institute of Standards and Technology, Gaithersburg, Maryland 20899 and Department of Materials and Nuclear Engineering, University of Maryland, College Park, Maryland 20742*

(Received 18 March 2002; published 27 September 2002)

The Heusler alloy Co_2MnSi is predicted to be a half-metallic ferromagnet and thus is considered a promising candidate for incorporation into spintronic devices. Recent theoretical calculations have shown that antisite disorder of a few percent in some Heuslers can destroy half metallicity, emphasizing the importance of characterizing samples for disorder. In this work we compare the magnetic, structural, and transport properties of Co_2MnSi for bulk single-crystal boules, polycrystalline arc-melted buttons and polycrystalline thin films. The lattice parameter, coercivity, and saturation magnetization of the single-crystal and arc-melted samples are statistically identical. On the other hand, the residual resistivity ratio $\rho_{300\,K}/\rho_{5\,K}$ shows sharp contrasts, with the single crystal and the arc-melted button having ratios of 6.5 and 2.7, respectively. Neutron-diffraction experiments show that the antisite disorder for the arc-melted samples is zero for Mn-Si antisite disorder, but between 10 and 14 % for Co-Mn antisite disorder. We postulate this to be the cause for the increased amount of defect-induced scattering in the electrical transport measurements of the arc-melted samples. The thin films, similarly, have lattice constants, magnetic properties, and room-temperature resistivities that approach those of the single crystal. The best films, however, have residual resistivity ratios of 1.4. By comparing these films to single crystalline thin films grown in other studies, we again find evidence supporting Co-Mn antisite disorder as the primary scattering mechanism.

DOI: 10.1103/PhysRevB.66.104429 PACS number(s): 72.25.Ba, 75.50.Cc, 75.70.−i

I. INTRODUCTION

Materials which display spin-polarized transport are of huge potential for various device applications.[1] Spin-polarized transport occurs when there is an imbalance between the densities of the two spin states in the conduction band. This imbalance has been successfully used for giant magnetoresistive read heads by the hard drive industry. In order to improve device performance, materials with a half-metallic band structure are sought. A half metal is a material with a gap between spin states at the Fermi level, such that the conduction electrons are entirely of one spin state.[2] In addition to improved read heads, such a material would be of great value in magnetically activated switches, magnetic field sensors, programmable nonvolatile memory, and other applications.

The primary figure of merit for magnetoresistive devices is the resistance ratio $\Delta R/R$, where ΔR is the resistance change between the parallel and antiparallel magnetization of adjacent magnetic layers in a multilayer device. According to the theory of Julliere the upper limit of $\Delta R/R$ in magnetic tunnel junctions is governed by the spin polarization (P) of the ferromagnetic materials used in the device.[3] Significant improvements in the processing of such devices will likely enhance $\Delta R/R$, however, the gains are expected to be incremental. Of the materials predicted to have half-metallic behavior, CrO_2 has been measured with a $P \sim 96\%$ and $La_{0.7}Sr_{0.3}MnO_3$ has been measured as high as $P = 90\%$ using Andreev reflection and 100% using spin-polarized photoemission.[4–6] Despite continuing efforts, integration of these materials into either spin valves or magnetic tunnel junctions has not yet been demonstrated and such achievements may take several years of intense development.

Another promising class of materials for spintronic applications is that of the Heusler alloys, a number of which have been predicted to be half-metallic ferromagnets.[2,7] These alloys have attractively high Curie temperatures (with the highest approaching 1000 K) and have been shown to have an integer number of Bohr magnetons per formula unit, which is a necessary, but not sufficient, condition for half metallicity. In addition, various studies have shown that these alloys can be processed as pure-phase thin films under conditions that are compatible with magnetoelectronic device manufacturing.[8,9]

It is therefore of concern that the performance of spin valves and magnetic tunnel junctions consisting of these alloys have displayed $\Delta R/R$ values far below those expected for a half metal.[10–12] Point contact spectroscopy on arc-melted specimens of NiMnSb measured P to be 58%,[13] indicating that the lack of half metallicity in these materials is indeed a bulk effect. Using first-principles band structure calculations on selected Heusler alloys, Orgassa *et al.* have shown that antisite disorder of only a few percent can destroy their half-metallic nature.[14]

In this work, we present a study of the structure, magnetism, and electronic transport for the Heusler alloy Co_2MnSi grown in a variety of ways. This ternary intermetallic is predicted to be half-metallic with a sizeable spin minority gap of 0.4 eV.[15] In addition, Co_2MnSi has a Curie temperature of 985 K, the highest amongst the Heusler alloys.[16] The high Curie temperature results in a flat temperature dependence of the magnetization for the temperature range of 5 to 300 K.

We begin with a description of the growth and character-

ization of high-quality, single-crystal boules (Sec. II). The study of these crystals allows us to establish benchmarks for resistivity, lattice constant, and magnetic properties with which to compare the arc-melted buttons and thin films grown by dc magnetron sputtering.

Section III details the growth and characterization of bulk, polycrystalline Co_2MnSi grown by arc melting of elemental constituents. The antisite disorder in these samples has been investigated using neutron diffraction. The results show that antisite disorder between the Co and Mn sublattices is prevalent while there is no measurable antisite disorder between the Mn and Si sublattices. Despite the disorder which is present, the arc-melted samples display magnetic and structural properties which are statistically equivalent to those of the single crystal. In contrast, the electrical transport properties are markedly different and we discuss the scattering mechanisms which are likely to be responsible.

In Sec. IV, the properties of thin film samples grown by dc magnetron sputtering are described. The best films exhibit magnetic and structural properties similar to those of the single crystal. In addition, these films have similar or higher residual resistivity ratios ($\rho_{300\,K}/\rho_{5\,K}$) than epitaxially grown single-crystal thin films of similar compositions.[17,18] However, the residual resistivity ratios are considerably lower than those of the single crystal and may be due to Co-Mn antisite disorder as was proposed for the bulk, arc-melted samples.

II. SINGLE CRYSTALLINE SAMPLES

Single crystal boules of Co_2MnSi were grown by the tri-arc Czochralski method. In this technique, a cylindrically shaped crystal is grown by slow pulling from a liquid melt of the desired stoichiometry. The melt was kept at temperature ($\sim$1523 K) by three arcs, formed under a positive pressure of Argon and spaced symmetrically around the melt. The liquid was continuously mixed in a rotating, water-cooled copper hearth while a seed crystal was rotated at 15 rpm in a direction counter to that of the hearth. Single crystals 30–40 mm in length were drawn at an optimal rate of 7 mm/h. Details on the preparation of the seed crystal and the melt can be found in Ref. 19.

The inset to Fig. 1 shows a single-crystal boule and the back-reflected Laue photograph along the (100) zone axis. Similar Laue patterns were observed at different positions along the length of the boule, thus confirming that the boule is single crystalline. Figure 1 shows the XRD pattern of a powdered single crystal.

Co_2MnSi has $L2_1$ crystal structure, which consists of a lattice with Mn on all face-centered cubic sites, Co on all tetrahedral sites, and Si on all octahedral sites. The XRD pattern for the powdered single crystal, shown in Fig. 1, displays all of the $L2_1$ peaks at their predicted intensities. The lattice constant for the sample is 5.654 ± 0.001 Å. The diffraction peak widths have been broadened by strain induced during the pulverization process.

Diffraction experiments on powders with the $L2_1$ structure yield two types of superlattice reflections in addition to the fundamental reflection. The diffraction peak for the (*h k l*) planes can be categorized as a type I superlattice reflection

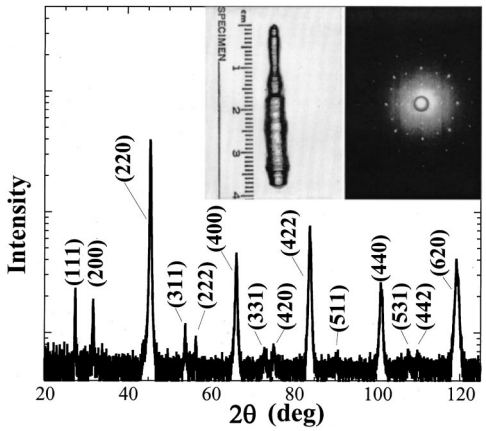

FIG. 1. X-ray diffraction pattern of powdered single crystal boule. Inset: photo of a boule and its corresponding back-reflected Laue photograph along the (100) zone axis.

when *h, k, l* are all odd [i.e., (111) peak], as a type II superlattice when *h, k, l* are all even and $h+k+l=2n$ [i.e., (200) peak], or as fundamental reflections where *h, k, l* are all even and $h+k+l=4n$ [i.e., (220) peak].[20] The ratio of superlattice intensity to principal peak intensity provides information regarding antisite disorder in the following ways: (1) disorder between Mn and Si sublattices reduces the type I superlattice peak to zero in the limit of complete disorder and (2) disorder between the Co and Mn sublattices reduces the intensities of type II superlattice peaks relative to that of the principal reflections. In practice, measuring disorder between the Co and Mn sublattices with XRD is extremely difficult. To understand why this is so, consider the scattering factors of Co and Mn atoms for the (111) peak when using Cu $K\alpha$ radiation. When both Thompson and anomalous scattering contributions are taken into account, the complex scattering factors are $15.61+3.62i$ and $15.52+2.81i$ for Co and Mn, respectively. Thus, the two atoms are nearly indistinguishable from the perspective of the standard XRD experiment.

Figure 2 shows a hysteresis loop of the single crystal as measured by superconducting quantum interference device (SQUID) magnetometry at 5 K. The coercive field is $\sim$5 Oe (see inset on the lower right) and the loop is canted as a result of the demagnetization field. The saturation magnetization of $5.10 \pm 0.04 \mu_B$ per formula unit is in good agreement with theoretical predictions of $5.0 \mu_B$ per formula unit.

The resistivity of the single crystal as a function of temperature is shown as an inset to Fig. 2 in the upper left of the figure. The crystal has a residual resistivity ratio (RRR) $\rho_{300\,K}/\rho_{5\,K}$ of 6.5, which is a very high RRR ratio for a ternary intermetallic. In general, the RRR is largest for metals whose temperature-dependent resistivities are dominated by phonon scattering contributions. However, small amounts of defects and impurities can have dramatic effects on this ratio as is well documented for metals such as copper. In ternary metals such as the Heuslers, a reduced RRR can result from scattering contributions from impurities or from antisite defects. Thus, we will refer back to RRR of the single crystal frequently as a benchmark with which to compare arc-melted and thin-film samples.

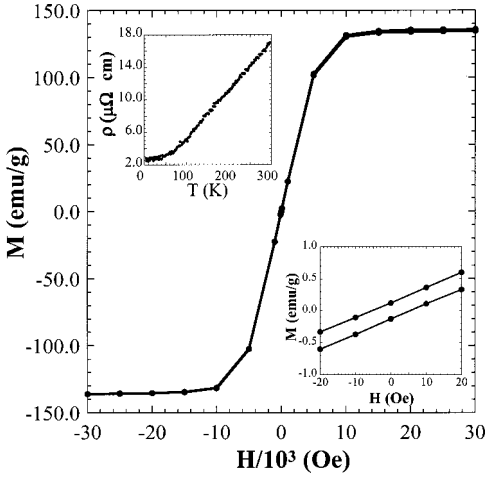

FIG. 2. Hysterisis loop of the single crystal at a temperature of 5 K. Lower right inset: low field portion of the hysterisis loop. Upper left inset: temperature dependence of the resistivity of the single crystal.

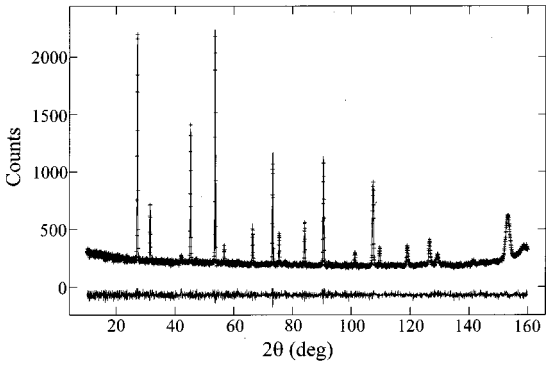

FIG. 3. The neutron-diffraction pattern of the arc-melted sample. The solid line is the fit to the data (crosses). The difference spectrum shown beneath the fitted data shows the excellent agreement of the model to the data.

III. ARC-MELTED SAMPLES

The structural and magnetic properties of pure-phase, arc-melted Co_2MnSi have been examined. Arc melting was performed using a water-cooled copper hearth under positive pressure of Ar. Elemental constituents of Co, Mn, and Si with purities of 99.9, 99.99, and 99.9995 %, respectively, were used as starting materials. A portion of the sample was powdered and used for XRD which confirmed that the ingot was single phase with an $L2_1$ crystal structure and a lattice constant of 5.654 ± 0.002 Å. The saturation magnetization was determined by SQUID magnetometry at 5 K to be $5.01 \pm 0.06 \mu_B$ per formula unit and the coercive field was ~5 Oe. Thus, characterization by XRD and SQUID magnetometry give statistically identical results for the single crystal and arc-melted sample (see Table I).

The temperature dependant resistivity, however, turns out to be quite different, with a RRR of 2.7 compared to the value of 6.5 for the single crystal. The arc-melted samples consist of large single crystalline grains, typically millimeters in diameter. Thus, contributions to the resistivity from grain-boundary scattering will be minimal, assuming their composition is not significantly different than that of the bulk. Since both the single crystal and the arc-melted sample are prepared under similar conditions (i.e., high temperatures of ~1500 K and a positive pressure of Ar) it is unlikely that defects due to impurities are the cause of the reduced RRR. This leaves antisite disorder as the most likely mechanism for the disparity between the arc-melt and single-crystal transport properties. In order to probe the antisite disorder of the ingot, neutron diffraction was employed to increase the Co/Mn contrast relative to XRD.

The neutron-diffraction measurements were made on arc-melted samples prepared under a variety of annealing and quenching conditions.[21] The diffraction data were measured using the BT-1 high-resolution powder diffractometer at the NIST Center for Neutron Research. The fit allows for varying degrees of antisite disorder between the Co, Mn, and Si sublattices (see Fig. 3). The data show that the Si site is fully occupied by Si, indicating that any antisite disorder in Co_2MnSi does not involve the Si atom. However, antisite disordering involving the Co and Mn sites is extensive with between 5 and 7 % of Co sites occupied by Mn atoms and, correspondingly, as much as 14% of Mn sites occupied by Co. As noted in Sec. II, Co/Mn antisite disorder is difficult to measure using XRD due to the similar x-ray scattering factors of Co and Mn. The neutron-scattering lengths of these atoms, however, are 0.253 and -0.373 for Co and Mn, respectively. As a result, disorder between the Co and Mn sublattices is easily identified, making neutron diffraction an ideal technique for evaluating this type of disorder in bulk samples.

IV. THIN FILM SAMPLES

Pure-phase thin films of Co_2MnSi were grown on glass substrates by dc magnetron sputtering in argon gas using 30

TABLE I. A comparison of structural, magnetic, and transport properties for Co_2MnSi.

Sample	Lattice constant (Å)	Saturation magnetization (μ_B per formula unit)	Coercive field (Oe)	Residual resistivity ratio ($\rho_{300\,K}/\rho_{5\,K}$)
Single crystal	5.654 ± 0.001	5.10 ± 0.04	5 ± 1	6.5
Arc-melted button	5.654 ± 0.002	5.01 ± 0.06	5 ± 1	2.7
Thin film ($P_{Ar} = 15$ mTorr, $T_D = 773$ K)	5.652 ± 0.002	4.90 ± 0.25	5 ± 2	1.4

TABLE II. Processing conditions of the polycrystalline thin films.

Sample	A	B	C	D	E	F
P_{Ar} (mTorr)	60	60	60	60	120	15
T_D (K)	423	573	673	773	773	773

W of dc power. The growth temperature ranged from 423 to 773 K and the growth pressure ranged from 15 mTorr to 120 mTorr (see Table II). The relatively thick (3.0 mm) magnetic target did not allow for a stable plasma below 15 mTorr. Films grown at or below 423 K have featureless XRD patterns except for a broad peak in the vicinity of the (220) peak. As shown in Fig. 4, films grown at or above 573 K are pure phase but unlike the single crystal, the superlattice peak intensities do not match theoretically predicted values. This can result from specific types of antisite disorder, as discussed in Sec. II, or from texturing. Figure 5 shows that texturing is indeed present by comparing the XRD pattern of film C before and after it has been rotated by $\psi = 45°$ about the *y* axis as defined in the diagram [Fig. 5(a)]. This is most evident in the (400) peak, which shows a significant enhancement in intensity after rotation. This texturing is a result of columnar-type growth as has been verified by TEM cross-sectional analysis [Fig. 5(b)].

Figure 6 shows the temperature dependence of the resistivity for the thin films and the single crystal. The thin films can be categorized as having high resistivities (i.e., those grown at 573 and 673 K) or having low resistivities (i.e., those grown at 773 K but at various pressures). The room-temperature resistivity of the best films approach that of the single crystal, however, the RRR ratio of the crystal is 6.5 versus 1.4 for the best film. One possible explanation is the presence of grain boundaries in the thin films, which becomes relevant when the mean free path of the electrons is a significant fraction of the grain diameter. However, our best

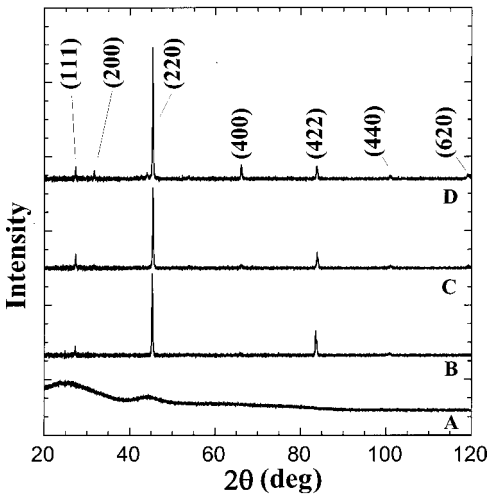

FIG. 4. X-ray diffraction patterns of films A–D, whose growth conditions are detailed in Table II. The broad peak at $2\theta \approx 25$ deg. for film A is due to the glass substrate. This peak has been subtracted from the patterns of films B, C, and D.

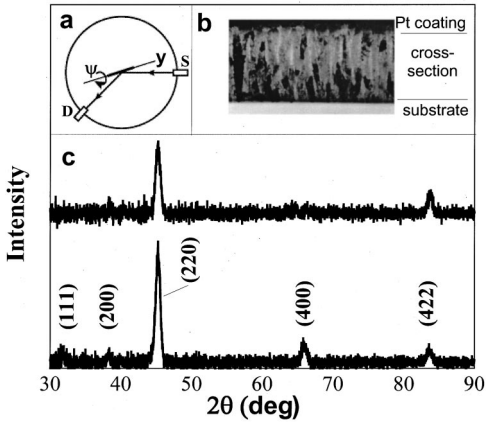

FIG. 5. Evidence of texturing in film C. (a) A diagram of the geometry used for investigating texture with the four-circle x-ray diffractometer, where *S* is the x-ray source and *D* is the detector. Scans were performed for various degrees of rotation about the *y* axis. (b) Cross-sectional TEM photograph revealing columnar-type growth. (c) X-ray diffraction scans for $\psi = 0°$ and $\psi = 45°$ rotation about the *y* axis.

films exhibit similar or higher RRR's than single crystalline thin films for alloys of similar composition.[16,18] This indicates that scattering due to grain boundaries does not play as large a role in reducing the RRR as that of scattering by impurities and antisite disorder in the films. We have also discussed in Sec. III the reduced RRR of the arc-melted sample relative to that single crystal and the neutron diffraction results, which showed the presence of 10–14 % disorder between the Co and Mn sites. In the arc melted samples, the growth temperatures are approximately 700 K higher than the thin film growth temperatures and there are no constraints imposed by a substrate. Therefore, it is reasonable to expect at least as much disorder for the thin films since the adatom mobilities in thin film growth are small compared to arc melting.

Figure 7 shows the RRR of the films and single crystal

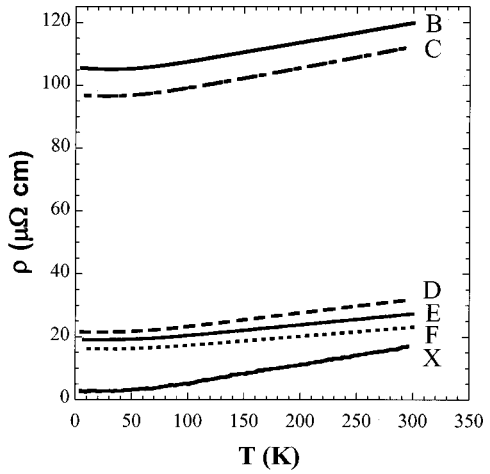

FIG. 6. The temperature-dependent resistivities of the thin films grown under a variety of temperature and pressure conditions (see Table II). For comparison, the temperature-dependent resistivity of the single crystal, denoted by *X*, is included.

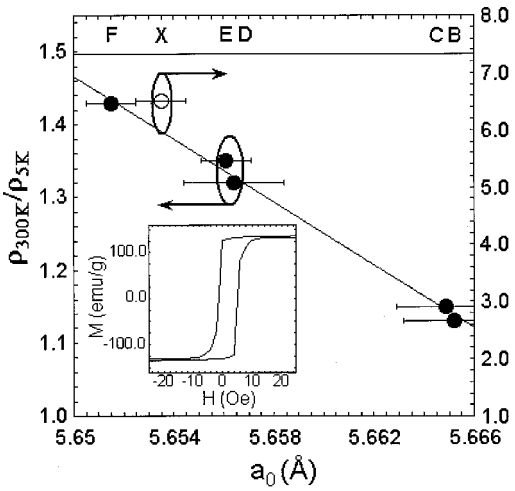

FIG. 7. The residual resistivity ratios versus lattice constant for the thin films (filled circles) and the single crystal (unfilled circle). The film corresponding to each data point (see Table II) is located directly above it. The single crystal is denoted by the letter *X* and its resistivity ratio is read from the ordinate scale on the right. Inset: the hysterisis loop of film F.

versus lattice constant. The lattice constants of the thin films approach that of the single crystal as the growth temperature of the films is raised and the Ar pressure is lowered. Film F, which was grown at 773 K and in 15 mTorr of Ar, has a lattice constant which is statistically equal to that of the single crystal. As shown in the inset to Fig. 7, these growth conditions also lead to magnetic properties which match those of the single crystal: a saturation magnetization and coercive field of $4.90 \pm 0.25 \mu_B$ per formula unit and ~ 5 Oe, respectively. Thus, our best films agree structurally and magnetically with single-crystal samples but differ dramatically when characterized by electronic transport. This suggests Co/Mn antisite disorder but requires independent verification.

V. CONCLUSIONS AND FUTURE WORK

In this work, we have compared the magnetic, structural, and transport properties of Co_2MnSi prepared as single crystals, arc-melted buttons, and polycrystalline thin films. Using the single crystal as a benchmark, we have found that both the arc-melted buttons and the thin-film samples can be grown with lattice constants, saturation magnetizations, and room-temperature resistivities which either closely approach or equal that of the single crystal. In contrast, the temperature-dependent resistivities are dramatically different, with the single crystal having a RRR which is 360% greater than that of our best thin films and 140% greater than that of the arc-melted button.

We have utilized neutron diffraction to measure significant levels of Co-Mn disorder in the polycrystalline bulk samples. First-principles band theory calculations have demonstrated that antisite disorder can destroy the half-metallic character of a number of Heusler alloys[14] and thus may be responsible for the low $\Delta R/R$ values reported for magnetoresistive devices which incorporate Heusler alloys. By comparing the transport properties of our polycrystalline thin films with those of the polycrystalline bulk samples and single-crystalline thin films, we have shown evidence that the antisite disorder may serve as the dominant electron-scattering mechanism in this alloy. This is only indirect evidence of disorder and emphasizes the importance of finding a technique which can be used to characterize antisite disorder in thin-film Heusler alloys. Recent measurements on thin films of Co_2MnGe show that such information can be obtained by the study of the diffraction anomolous fine structure.[22]

ACKNOWLEDGMENTS

We gratefully acknowledge E. E. Carpenter, I. I. Mazin, and T. O'Brian for helpful discussions and assistance. This work has been supported by the Office of Naval Research.

[1] G. A. Prinz, Science **282**, 1660 (1998).
[2] W. E. Pickett and J. S. Moodera, Phys. Today **54**, 39 (2001).
[3] M. Julliere, Phys. Lett. **54A**, 225 (1976).
[4] Y. Ji, G. J. Strijkers, F. Y. Yang, C. L. Chien, J. M. Beyers, A. Anguclouch, Gang Xiao, and A. Gupta, Phys. Rev. Lett. **86**, 5585 (2001).
[5] B. Nadgorny, I. I. Mazin, M. Osofsky, R. J. Soulen, Jr., P. Broussard, R. M. Stroud, D. J. Singh, V. G. Harris, A. Arsenov, and Ya. Mukovskii, Phys. Rev. B **63**, 184433 (2001).
[6] R.-H. Park, E. Vescovo, H.-J. Kim, C. Kwon, R. Ramesh, and T. Venkatesan, Nature (London) **392**, 794 (1998).
[7] V. Y. Irkhin and M. I. Katsnel'son, Usp. Fiz. Nauk **164** (7), 705 (1994) [Phys. Usp. **37** (7), 659 (1994)].
[8] M. P. Raphael, B. Ravel, M. A. Willard, S. F. Cheng, B. N. Das, R. M. Stroud, K. M. Bussmann, J. H. Claassen, and V. G. Harris, Appl. Phys. Lett. **79**, 4396 (2001).
[9] J. A. Caballero, Y. D. Park, A. Cabbibo, J. R. Childress, F. Petroff, and R. Morel, J. Appl. Phys. **81**, 2740 (1997).
[10] C. T. Tanaka, J. Nowak, and J. S. Moodera, J. Appl. Phys. **86**, 6239 (1999).
[11] T. Ambrose, J. J. Krebs, and G. A. Prinz, J. Appl. Phys. **89**, 7522 (2001).
[12] C. Hordequin, J. P. Nozières, and J. Pierre, J. Magn. Magn. Mater. **183**, 225 (1998).
[13] R. J. Soulen Jr., J. M. Beyers, M. S. Osofsky, B. Nadgorny, T. Ambrose, S. F. Cheng, P. R. Broussard, C. T. Tanaka, J. Nowak, J. S. Moodera, A. Barry, and J. M. D. Cooey, Science **282**, 85 (1998).
[14] D. Orgassa, H. Fujiwara, T. C. Schulthess, and W. H. Butler, Phys. Rev. B **60**, 13 237 (1999).
[15] S. Ishida, T. Masaki, S. Fujii, and S. Asano, Physica B **239**, 163 (1997).
[16] P. J. Brown, K. U. Neumann, P. J. Webster, and K. R. A. Ziebeck, J. Phys.: Condens. Matter **12**, 1827 (2000).
[17] T. Ambrose, J. J. Krebs, and G. A. Prinz, Appl. Phys. Lett. **76**, 3280 (2000).

[18] R. Remesh and V. Saraf (private communication).
[19] S. F. Cheng, B. Nadgorney, K. Bussmann, E. E. Carpenter, B. N. Das, G. Trotter, M. P. Raphael, and V. G. Harris, IEEE Trans. Magn. **37**, 2176 (2001).
[20] P. J. Webster, J. Phys. Chem. Solids **32**, 1221 (1971).
[21] B. Ravel, M. P. Raphael, V. G. Harris, and Q. Huang, Phys. Rev. B **65**, 184431 (2002).
[22] B. Ravel, J. O. Cross, M. P. Raphael, V. G. Harris, R. Ramesh, and V. Saraf, Appl. Phys. Lett. (to be published).